Available online at www.sciencedirect.com

ScienceDirect

Palaeoworld 35 (2026) 200996

Palaeoworld

www.elsevier.com/locate/palwor

New *Pachyportax* fossils from the Late Miocene Shuitangba locality, Yunnan, revealing the early Bovini evolution and radiation

Ding-Ge Guo [a,b], Sayyed Ghyour Abbas [c], Qi-Gao Jiangzuo [a], Chun-Xiao Li [a,b], Yan-Wu Yang [d], Jia-Yong Cao [d], Bin Zou [e], Shi-Qi Wang [a,*], Xue-Ping Ji [f,*]

[a] *Key Laboratory of Vertebrate Evolution and Human Origins, Institute of Vertebrate Paleontology and Paleoanthropology, Chinese Academy of Sciences, Beijing 100044, China*

[b] *University of Chinese Academy of Sciences, Beijing 100049, China*

[c] *University of Sialkot, Sialkot, Punjab 51040, Pakistan*

[d] *Zhaotong Institute of Cultural Relics Protection and Archaeology, Zhaotong 657000, China*

[e] *Zhaoyang Museum, Zhaotong 657000, China*

[f] *Natural History Museum of Zoology, Kunming Institute of Zoology, Chinese Academy of Sciences, Kunming 650201, China*

Received 13 February 2025; received in revised form 29 May 2025; accepted 16 July 2025
Available online 22 July 2025

Abstract

As a small-sized Bovini, *Pachyportax*, originated in the Late Miocene Siwaliks and subsequently dispersed to neighbouring regions in Southeast Asia and the Arabian Peninsula, and eventually reached Yunnan, China. However, no fossil material of this genus had been discovered in China prior to this study. Here we report a new species *Pachyportax zhaotongensis* n. sp., from an important fossil ape locality, the Shuitangba site in Zhaotong, Yunnan, China, dated at approximately 6.2 Ma. The new species displays the diagnostic characteristics of *Pachyportax*, such as a robust horn core that extends laterally and backward, with a slightly convex medial side and a flatter lateral side, featuring anterior and posterior keels; the cheek teeth are hypsodont, with moderately developed ribs, folds and basal pillars. It also shows some differences from the known species: the horn core insertion is distant from the orbit and shows no significant torsion, and the anterior and posterior keels on the horn core are less pronounced. These advanced characteristics indicated that *Pachyportax zhaotongensis* n. sp. represents a late evolutionary stage of *Pachyportax*. This is also the first report of *Pachyportax* in China. In addition, based on a phylogenetic analysis, we clarify the relationship of *Selenoportax* and *Pachyportax*, and briefly explore the evolution and geographical distribution of the two genera.

Keywords: Zhaotong; Late Miocene; *Selenoportax*; *Pachyportax*; Phylogenetic analysis; Biogeography

1. Introduction

The members of the family Bovidae (sheep, goats, buffalo, cow, etc.) are among the most widespread groups worldwide, have a long domestication history, and an extensive fossil record (Renfrew, 2006; Bibi, 2007; Bibi et al., 2009; Zhang et al., 2020). Their fossil record dates back to the lowest Miocene (~23 Ma), and the subfamily Bovinae is represented by many fossil taxa (Gentry et al., 1999; Bibi et al., 2009; Nishioka et al., 2019, 2020). Despite their extensive fossil record, their phylogenetic relationships and biogeographic history are not yet fully resolved,

* Corresponding authors.
E-mail addresses: wangshiqi@ivpp.ac.cn (S.Q. Wang), jxpchina@foxmail.com (X.P. Ji).

https://doi.org/10.1016/j.palwor.2025.200996

Fig. 1. A map showing the location of the Shuitangba yielding the specimens described in this study.

and this is especially true for the members of the tribe Bovini. The members of this tribe are known from Eurasia (Lyman, 2004; Martínez-Navarro and Palombo, 2004; Khan et al., 2009, 2012; Martínez-Navarro et al., 2011; Siddiq et al., 2016; Tong et al., 2017), America (Froese et al., 2017) and Africa (Gentry and Gentry, 1978; Gentry et al., 1999, 2014; Harris, 2003; Bibi, 2007; Bibi et al., 2009). The taxonomic status of some members of this tribe is controversial as they have been placed in different taxonomic categories. For example, *Pachyportax* and *Selenoportax*, commonly found in the Siwalik Group of the Indian subcontinent (Pilgrim, 1937, 1939; Akhtar, 1992; Bibi, 2007; Khan et al., 2009; Abbas et al., 2018), were previously treated as boselaphines for a long time and recently Bibi (2007) suggested their attribution to tribe Bovini. These genera date back to 10.2 Ma from the Siwaliks (Gentry et al., 2014, 2025). Besides the Siwaliks of the Indian subcontinent, the fossils of *Pachyportax* and *Selenoportax* are known from the Arabian Peninsula (Gentry, 1999; Bibi, 2022a), Thailand (Nishioka et al., 2020), and Myanmar (Nishioka et al., 2019), while *Selenoportax* is reported from Yunnan, China (Han, 1985; Qiu and Qiu, 1995). Although Han (1985) and Qiu and Qiu (1995) reported the presence of *Selenoportax* sp. from Lufeng, Yunnan, China, no illustrations were published. As a result, confirmation of its presence, and the evolution of early Bovini in China remains poorly understood.

In this study we describe some fossils of the genus *Pachyportax* from China for the first time and provide a complete phylogenetic analysis of tribe Bovini to demonstrate the relationship of *Selenoportax* and *Pachyportax*.

2. Geographic and geological settings

The Shuitangba site (27°19'44"N, 103°44'15"E, 1918 masl) in Zhaotong, Yunnan, China, is located in the Zhaotong Basin in the northeastern part of Yunnan Province (Fig. 1). This site is an open-air lignite coal seam belonging to the Zhaotong Formation, which dates from the late Miocene to the Pliocene (8.8–2.6 Ma). This formation mainly consists of lacustrine clay, silt, lignite, and carbonaceous clay. At the Shuitangba outcrop, a sequence of seven sedimentary layers can be observed, with a total thickness of 16 m (Ji et al., 2013; Chang et al., 2015; Zhang et al., 2016a; Huang et al., 2017; Sun et al., 2021). In terms of age, the Shuitangba mammalian assemblage can be reliably correlated to the Dhok Pathan Formation of the Siwaliks (7.2–5.3 Ma). Our fossil material was collected from the

fine, dark clay layers between the Lignite Seams, palaeomagnetically dated to ~6.2 Ma (Ji et al., 2013; Jablonski et al., 2014; Sun et al., 2021).

3. Material and methods

3.1. Material

The material includes ten specimens comprising of a partial cranium with horn core, a mandibular fragment, and isolated upper and lower teeth.

3.2. Measuring methods and nomenclature

Measurements of the skulls and teeth were taken using a digital caliper (Delixi Electric) and software programs Meshlab (v2022.02) and 3-matic Research (v11.0). For the teeth, the maximum crown length and crown width (at the base of the crown) were measured, and the crown height was measured from the part below the protocone/protoconid to the base of the crown. The cross sectional measurements of the horn cores refer to Nishioka et al. (2020). Dental terminology follows Bärmann and Rössner (2011) with slight modification, as given in Fig. 2.

3.3. Cladistic methodology

To determine the phylogenetic position of our material, we conducted a phylogenetic analysis. The data matrix contains 32 taxa, in which *Boselaphus tragocamelus*, an extant boselaphine, was selected as the outgroup, and the remaining 31 taxa include all the major Bovini clades. The morphological characters encompassed 162 characters from the skull (Bibi, 2009). The cladogram was reconstructed using Bayesian tip dating (BTD). The data set was used when performing the Bayesian total-evidence dating analysis (Ronquist et al., 2012a; Gavryushkina et al., 2014; Zhang et al., 2016b), in which the fossil ages were incorporated as tip calibrations. The Lewis Mkv model (Lewis, 2001) with gamma rate variation across characters (Yang, 1994) (Mkv + Γ) was used for the morphological characters. The prior for the timetree was modelled by the fossilized birth-death process (Stadler, 2010; Heath et al., 2014). The process is conditioned on the time of the most recent common ancestor (root age) and has hyperparameters of speciation rate, extinction rate, fossil-sampling rate, and extant-sampling probability. The root age was assigned an offset-exponential prior with mean age of 15 Ma and minimal age of 13 Ma, referring to the mitochondrial phylogenetics calibrated by fossil records (Bibi, 2013). The ages of the fossils were given uniform distributions based on their related stratigraphic ranges. The extant-sampling probability was fixed to 0.3 based on the number of relevant living genera. Apart from the timetree, the other key component is the relaxed clock model, which models the evolutionary rate variation along the branches in the tree. We used the independent gamma rate clock model (Lepage et al., 2007), in which the mean clock rate was assigned a lognormal (–6, 1) prior and the variance parameter of the clock rate was exponential (10). We executed two independent runs and four chains per run (one cold chain and three hot chains) in the Markov chain Monte Carlo simulation. Each run was executed 1 million generations and sampled every 1000 generations. The first 25% samples were discarded as burn-in and the rest from the two runs were combined. Good convergence and mixing were diagnosed by the effective sample size (Geyer, 1992) larger than 200 for all parameters and the average standard deviation of split frequencies (Ronquist et al., 2012a) smaller than 0.01. The BTD analysis was performed in MrBayes 3.2.7 (Ronquist et al., 2012b), see Supplementary data. The node supports were shown using post-probabilities.

3.4. Comparative material and repository

Comparative materials were obtained from the American Museum of Natural History (AMNH), and other materials were sourced from the literature. The studied material is preserved in the Zhaoyang District Museum (ZYM), Zhaotong City, Yunnan Province.

4. Systematic palaeontology

Family Bovidae Gray, 1821
Subfamily Bovinae Gray, 1821
Tribe Bovini Gray, 1821
Genus *Pachyportax* Pilgrim, 1937

Pachyportax zhaotongensis n. sp.
(Figs. 2–4)

Etymology: The species name derives from the locality, Zhaotong.
Holotype: ZYM ZT-2015-01461, a partial cranium with complete right horn core.
Paratype material: ZYM ZT-2015-02328, a left P3; ZYM ZT-2015-02157, a right P4; ZYM ZT-2015-02328, a left M2; ZYM ZT-2015-0219, left i1; ZYM ZT-2015-02308, left i1; ZYM ZT-2015-01643, a fragmentary juvenile left mandible bearing dp3, dp4, and m1 and alveoli of dp2; ZYM ZT-2015-0072, a right p4; ZYM ZT-2015-0576, a left m3.
Type locality and age: Shuitangba site, belonging to the Zhaoyang District of the Zhaotong City, Yunnan Province, Late Miocene, estimating ~6.2 Ma.
Diagnosis: A medium sized species of the genus, slightly larger than *P. nagrii*; horn core robust, slightly distantly inserted on the orbit, extending laterally and backward, with a convex medial side and a flatter lateral side, featuring less sharp anterior and posterior keels; hypsodont cheek teeth, with moderately developed ribs, folds and basal pillars.
Differential diagnosis: Differentiated from *P. nagrii* in having slightly larger size, more robust horn core and weaker keels; differentiated from *P. latidens* and *P. giganteus* in

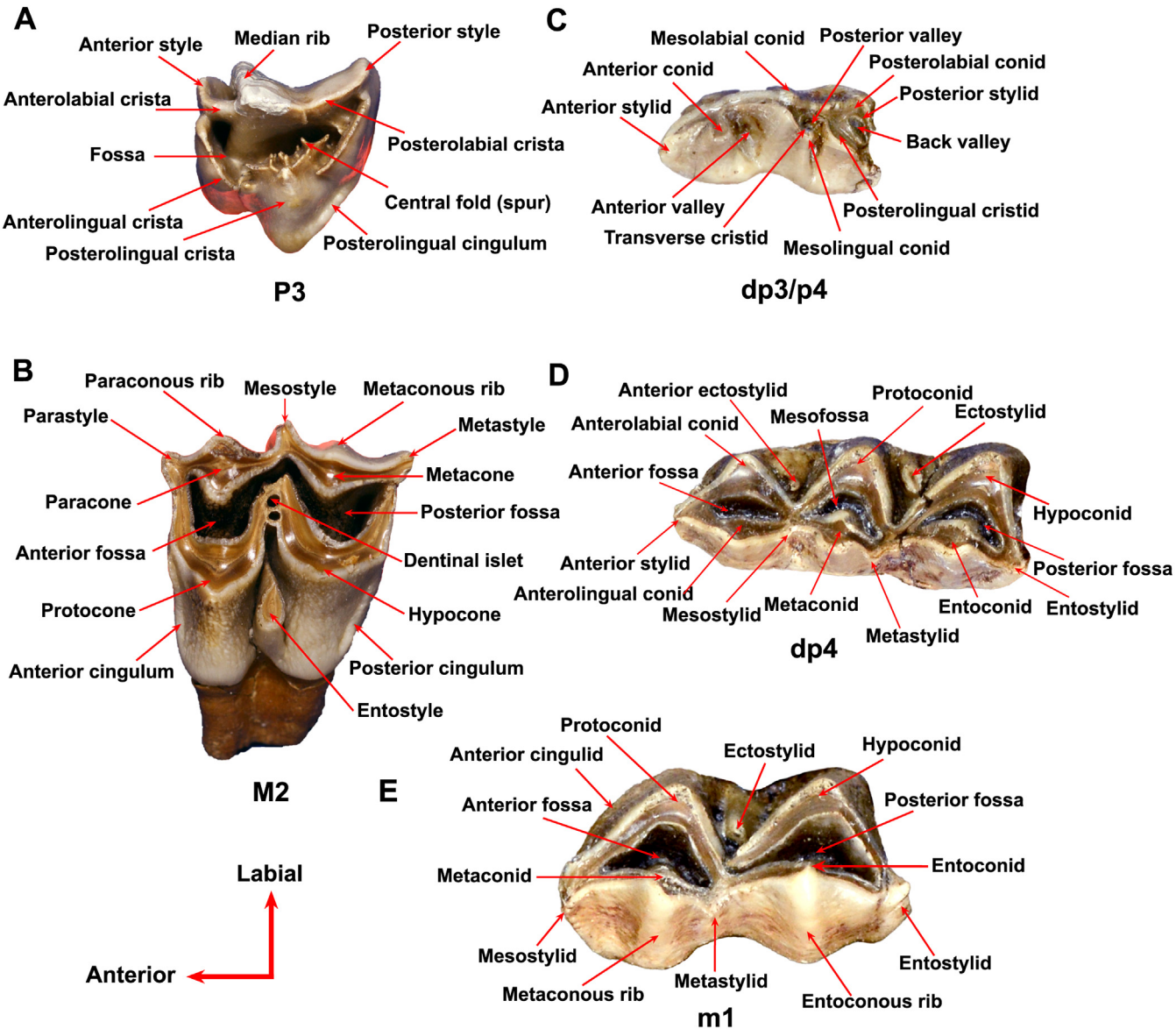

Fig. 2. Terminology of bovid teeth (after Bärmann and Rössner, 2011). (A) Left P3. (B) Left M2. (C) Left dp3/right p4. (D) Left dp4. (E) Left m1. Not to scale

smaller size, horn core with weaker keels and having greater distance between the orbit and the horn core.

Description:

ZYM ZT-2015-01461 (Fig. 3) is a partial cranium with right horn core. The horn core pedicle was damaged during excavation, making it difficult to repair accurately. In the current stage, the horn core is closer to the mid-sagittal plane than it should be. The horn core surface is marked by numerous large vascular foramina with fine vascular grooves, and the longitudinal rigids are not prominent. This morphology indicates that it is a sub-adult individual. The horn core is robust and long, extending posterolaterally and slightly curving upwards, with a bend towards the midline at about one fourth from the tip. The horn core exhibits a faint anticlockwise spiral morphology (proximal view) bearing three longitudinal keels: the moderately developed anteromedial and posteromedial keels collectively form the convex medial surface, while the lateral surface shows reduced convexity due to the presence of a subtle third keel. This keel merges with the anteromedial keel at the distal one fourth of the horn core. The cross section at the base is ovoidal triangular or subtriangualr, being convex on the medial and partly flat on the lateral. The pedicle is damaged but is relatively long, the frontal sinus extends deeply into the horn core observed from the broken cortical bones. The remaining frontal is severely damaged. A prominent keel extending from the anterior base of the horn pedicle to the frontal, dividing the latter into two parts. The ventral surface of the frontal

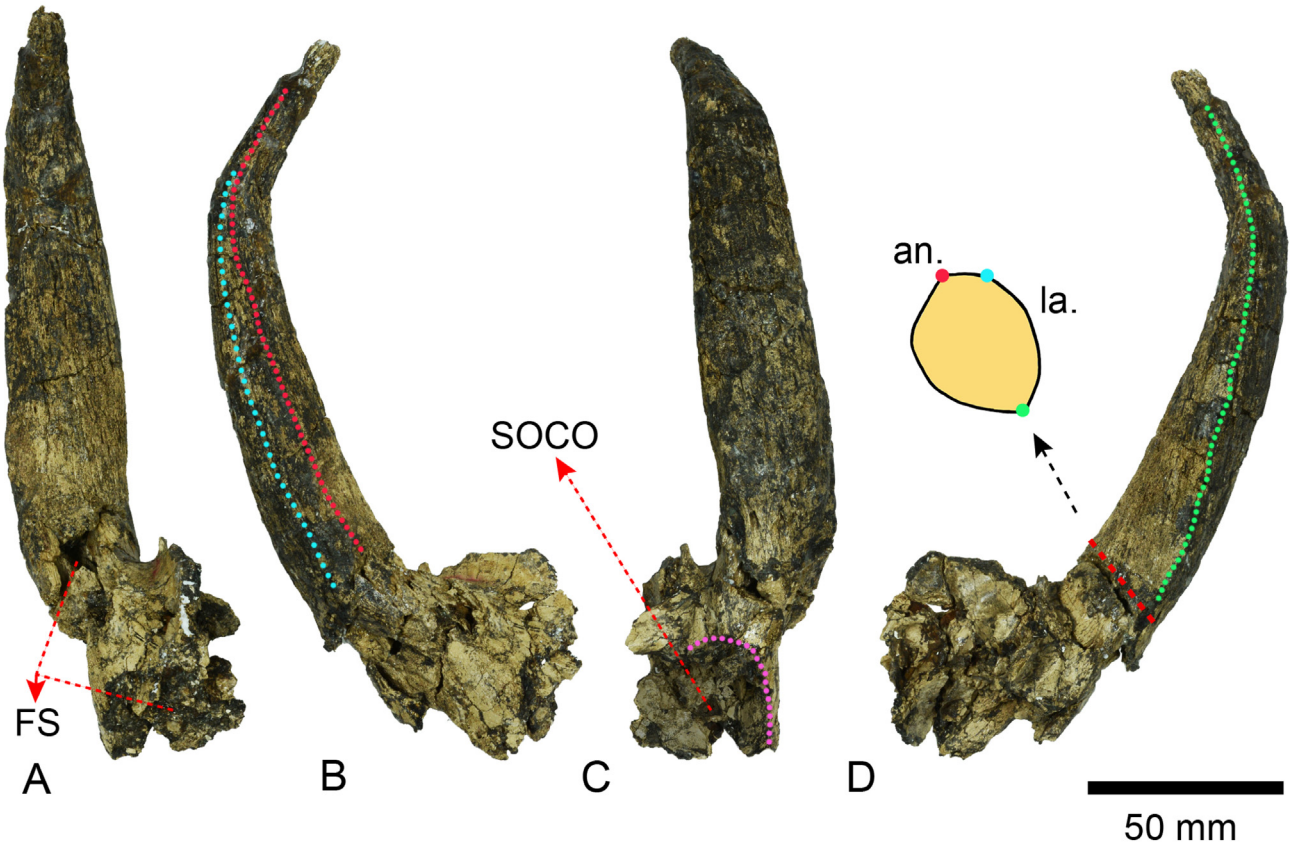

Fig. 3. Holotype of *Pachyportax zhaotongensis* n. sp. ZYM ZT-2015-01461, a partial cranium with complete right horn core. (A) Medial. (B) Anterior. (C) Lateral. (D) Posterior views. FS, frontal sinus; SOCO, opening of the supraorbital channel in the orbit; the pink dashed line is labeled outlines the orbit. The red dashed line denotes the anteromedial keel, the green one, the posteromedial keel, and the blue one, the third keel. In the cross-section of the horn core, the red, green, and the blue points represent the position of the anteromedial, posteromedial, and third keels, respectively. Abbreviations: an, anterior; la, lateral.

shows complicated impressions made by the convolution of the brain. The orbits are anteriorly positioned relative to the horn core insertion, and the supraorbital channel is recognizable, although it is not very clear for the damage of the adjacent bones. The frontal bone is thickened due to the development of the frontal sinus. Measurements are given in Table 1.

Upper dentition: The upper cheek teeth are represented by isolated P3, P4 and M2.

ZYM ZT-2015-02328 is an unworn P3 (Fig. 4A) in which the apex of the median rib is damaged due to isotope sampling done by Sun et al. (2021). In occlusal view, the shape is approximately rectangular, showing a very complex internal fold structure. The labial surface is relatively flat, while the lingual surface is rounded. The anterior lingual cone is small and is separated from the posterior lingual cone by a prominent groove. The posterior lingual cone projects strongly lingually and its buccal wall bears several small folds (spurs) extending towards the fossa. The anterolingual cone and the anterior style, as well as the posterolingual cone and the posterior style are connected to each other. Both the anterior style and the posterior style are well developed, the anterior style projects buccally, and the posterior style projects posterolabially. The buccal side is divided into anterolabial cone and posterolabial cone as well as median rib. It is positioned anteriorly, and swells in both buccal and lingual directions, while more prominent in buccal direction. In the buccal view, the crown is high, showing three columns of the anterior and posterior styles and the median rib. The column of the anterior style and the median rib are connected at the crown base, forming a V-shape (Fig. 4A2). A thick posterolingual cingulum is present at the base of the tooth. The median rib exhibits pathological features, with the enamel displaying arranged crest and trough pattern consistent with enamel hypoplasia and hyperplasia. The tooth is supported by three roots, two buccal and one lingual where the distobuccal root is better preserved.

ZYM ZT-2015-02157 represents a P4 (Fig. 4B). It is in late wear. In occlusal view, the shape is nearly triangular, with the length slightly smaller than the width (Table 2). The lingual wall is round, while the buccal wall is flat. The labial cones swell both buccally and lingually; the anterior style is small and projects buccally, the posterior style is large while the median rib is thick at the base and gradually becomes thin and small towards the apex. A prominent spur is present in the outer wall of fossa anteriorly. In the buccal view, the crown is high, and the buccal cones

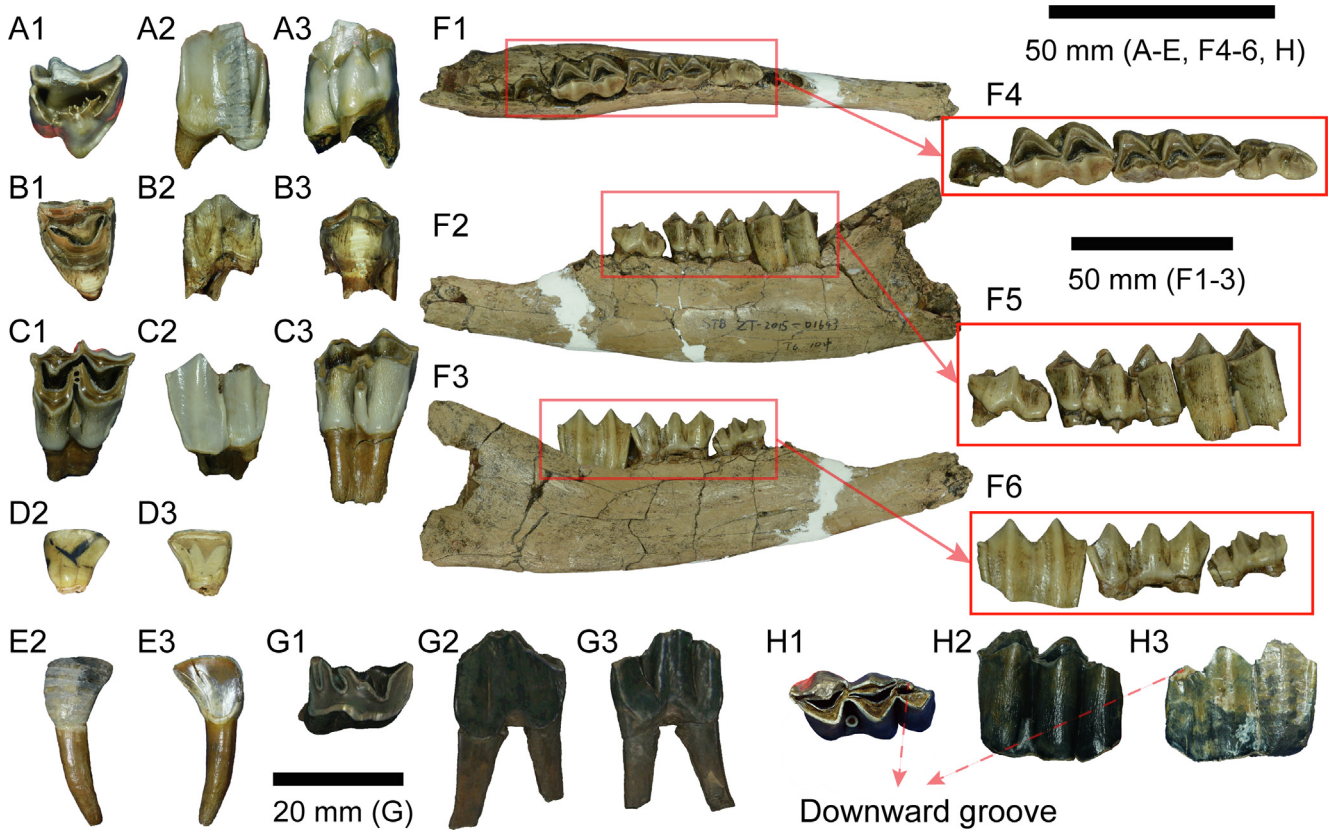

Fig. 4. Cheek teeth of *Pachyportax zhaotongensis* n. sp. (A) ZYM ZT-2015-02328, left P3. (B) ZYM ZT-2015-02157, right P4. (C) ZYM ZT-2015-02328, left M2. (D) ZYM ZT-2015-02308, left i1. (E) ZYM ZT-2015-02129, left i1. (F) ZYM ZT-2015-01643, a fragmentary juvenile left mandible bearing dp3, dp4, and m1. (G) ZYM ZT-2015-0072, right p4. (H) ZYM ZT-2015-0576, left m3. (1. occlusal view; 2. buccal view; 3. lingual view).

Table 1
Comparative measurements (in mm) of horn core of *Pachyportax zhaotongensis* n. sp. with other species of the genus *Pachyportax*.

Species	Anteroposterior diameter (DAP)	Transverse diameter (DT)
P. zhaotongensis n. sp.	50.78 (ZYM ZT-2015-01461, this study)	34.11 (ZYM ZT-2015-01461, this study)
P. nagrii	46 (AMNH 19764, Pilgrim, 1937)	30 (AMNH 19764, Pilgrim, 1937)
P. latidens	56 (GSI-B 488, Pilgrim, 1937)	42 (GSI-B 488, Pilgrim, 1937)
	62 (PUPC 85/103, Akhtar, 1992)	48 (PUPC 85/103, Akhtar, 1992)
	59 (PUPC 85/104, Akhtar, 1992)	45 (PUPC 85/104, Akhtar, 1992)
P. giganteus	78 (PUPC 87/323, Akhtar, 1992)	52 (PUPC 87/323, Akhtar, 1992)
	79.8 (TKK 61, Nishioka et al., 2020)	52.7 (TKK 61, Nishioka et al., 2020)
	84.7 (TKK 153, Nishioka et al., 2020)	60.1 (TKK 153, Nishioka et al., 2020)

show an upward apex. The three columns of the anterior style, the median rib and the posterior style are all observed and the former two are fused at the crown base. The enamel is moderately rugose.

ZYM ZT-2015-02328 is an isolated well preserved M2 (Fig. 4C). The tooth has two lobes and shows significant wear. The enamel is moderately rugose. In occlusal view, the shape is nearly square, with the length slightly greater than the width (Table 2). The protocone is narrow due to the pinching of pre- and postprotocrista making a pointed apex, while the metaconule is broader than the protocone having a round lingual wall. The entostyle is well developed and thick. It is tall in lingual and occlusal views and forms a droplet shape with a buccal sharp apex. The parastyle is small and projects anteriorly; the paracone is large and inflate both lingually and buccally; the mesostyle projects prominently towards the buccal side; the metacone is larger with a prominent lingual inflation and a weaker buccal inflation; and the metastyle is smaller and projects posteriorly. Two dentinal islets are present between the buccal borders of postprototocrista and premetaconulecrista. In buccal view, the metacone protrudes upwards to form a triangle. The columns of the parastyle, the mesostyle, and the metastyle are sharp, while that of rib of the paracone and

Table 2
Comparative measurements (in mm) of the cheek teeth of different species of the genus *Pachyportax*. Abbreviations: L, tooth crown length; W, tooth crown width; W/L, the width to length ratio.

Species	Locus/specimen number	L (mm)	W (mm)	W/L	Reference
Pachyportax zhaotongensis n. sp.	P3 (ZYM ZT-2015-02328)	21.78	22.24	1.02	This study
	P4 (ZYM ZT-2015-02157)	17.58	21.25	1.21	This study
	M2 (ZYM ZT-2015-02328)	23.46	25.09	1.07	This study
	dp3 (ZYM ZT-2015-01643)	17.84	9.55	0.54	This study
	dp4 (ZYM ZT-2015-01643)	26.02	11.91	0.46	This study
	p4 (ZYM ZT-2015-0072)	18.43	10.57	0.57	This study
	m1 (ZYM ZT-2015-01643)	24.81	10.25	0.41	This study
	m3 (ZYM ZT-2015-0576)	32.63	15.65	0.48	This study
Pachyportax latidens	P3 (GSI-B 218)	19.00	19.00	1.00	Pilgrim (1937)
	P4 (GSI-B 218)	16.00	19.50	1.22	Pilgrim (1937)
	M2 (GSI-B 218)	25.00	26.00	1.04	Pilgrim (1937)
	M2 (AMNH 29964)	28.00	25.00	0.89	Pilgrim (1937)
	M2 (AMNH 19730)	28.50	28.50	1.00	Pilgrim (1937)
	M2 (AMNH 19841)	25.00	26.00	1.04	Pilgrim (1937)
	m1 (GSI-B 268)	24.00	10.00	0.42	Pilgrim (1937)
	M2 (PUPC 96/3)	27.00	22.00	0.81	Khan et al. (2009)
	M2 (PUPC 86/37)	27.40	18.00	0.60	Khan et al. (2009)
	M2 (PUPC 86/36)	30.00	23.00	0.70	Khan et al. (2009)
	M2 (PUPC 83/718)	27.40	26.00	0.90	Khan et al. (2009)
	M2 (PUPC 83/646)	30.0	18.00	0.60	Khan et al. (2009)
	M2 (PUPC 83/744)	30.20	21.90	0.72	Khan et al. (2009)
	m3 (PUPC 04/16)	34.00	17.30	0.50	Khan et al. (2009)
	m3 (PUPC 86/7)	33.00	14.00	0.40	Khan et al. (2009)
	m3 (PUPC 96/41)	38.00	16.30	0.42	Khan et al. (2009)
	P3 (PUPC 86/215)	18.50	20.40	1.10	Akhtar (1992)
	P4 (PUPC 86/215)	16.30	21.60	1.33	Akhtar (1992)
	M2 (PUPC 86/215)	26.00	28.00	1.08	Akhtar (1992)
	M2 (PUPC 04/31)	26.00	26.00	1.00	Babar et al. (2018)
	M2 (PUPC 07/166)	28.00	26.00	0.93	Babar et al. (2018)
	m3 (PUPC 13/234)	40.00	19.00	0.48	Babar et al. (2018)
	p4 (PC-GCUF 11/82)	20	13	0.65	Abbas et al. (2018)
	m1 (PC-GCUF 11/82)	21	15	0.71	Abbas et al. (2018)
	m3 (PC-GCUF 11/82)	36	18	0.50	Abbas et al. (2018)
Pachyportax nagrii	M2 (PUPC 04/3)	23.00	23.00	1.00	Babar et al. (2018)
	M2 (PUPC 13/287)	24.00	21.80	0.91	Babar et al. (2018)
	M2 (PUPC 69/206)	18.50	16.00	0.86	Babar et al. (2018)
	M3 (GSI-B 808)	19.00	14.00	0.74	Babar et al. (2018)
	M1 (PUPC 86/77)	21.00	21.40	1.02	Babar et al. (2018)

the metacone are blunt but thick. The anterior cingulum is much thicker than the posterior cingulum.

Lower dentition: The lower dentition is represented by two isolated i1s, a juvenile hemimandible, along with an isolated p4 and m3.

ZYM ZT-2015-02308 (Fig. 4D) and ZYM ZT-2015-0219 (Fig. 4E) are two isolated left i1s, and the later retains a slender, conical root. Both are flat, shovel-shaped, with a sharp distal angle and a rounded mesial angle. The dorsal edge is sharp, the labial surface is convex, and the lingual surface is straight. There is a narrow and long wear facet longitudinally on the lingual side. A small ridge divided the crown into anterior and posterior half lingually.

ZYM ZT-2015-01643 (Fig. 4F) is a juvenile left hemimandible with the ascending ramus missed while the diastema is preserved. It bears the dp3-dp4, m1, anterior lobe of erupting m2 and alveoli of dp2. The dp2 is shed leaving only alveoli, the p2 has not erupted yet, and the m2 is in eruption. The mandibular is robust. It is deep in the lateral view and wide in dorsal view. The diastema is not very long. The mental foramen is present deeply under dp3. It is compressed dorsoventrally and extended anteroposteriorly.

The outline of the dp3 (Fig. 4F) is narrow and elongated (approximately twice as long as wide; Table 2). It is moderately worn. In occlusal view, the mesolabial conid is large and rounded, while the posterolabial conid is smaller, with a more pronounced projection than that of the mesolabial conid. They are separated by a weak groove. On the lingual side, the anterior stylid and the anterior conid are bifurcated. The former is slender and mesially projected, and the latter is short, pointing towards the lingual side; the

mesolingual conid is joined to the mesolabial conid through a transverse cristid, featuring a posterolingual cristid that inclines posterolingually. The posterolingual conid is large and rounded, and the posterior stylid forms a cristid, encircling the back of the tooth. It merges with the posterolingual conid and closes off the back valley. Anterior valley is widest and open lingually. In lateral view, the posterior conid shows a shape apex.

The dp4 (Fig. 4F) is in moderate wear and trilobed. It is approximately three times longer than wide (Table 2). The anterior ectostylid and the ectostylid are well-developed (the latter being more robust), cone shaped. In occlusal view, the first lobe is rhomboid, while the posterior two lobes are nearly triangular. All cristids between the lobes and at the mesial and distal extremities are interconnected due to the moderate wear. For the anterolabial conid, protoconid, and hypoconid, each has a buccal angle, with the latter in turn more buccally projected than the former. The anterior stylid projects mesially. The anterolingual conid, metaconid, and entoconid, all swell in both buccal and lingual sides. The metastylid is nearly absent, the mesostylid is weak, and the entostylid is larger, projecting distally. The anterior valley is the widest and opens lingually. In lingual view, the crown is significantly lower than that of the molars; the anterolingual conid, metaconid, and entoconid show three upward apices, with the ribs of each being thick and columnar. The columns of the anterior stylid and entostylid are thinner.

The m1 (Fig. 4F), is in slight wear, with a length approximately twice the width (Table 2). In occlusal view, both lobes are triangular. The anterior lobe is slightly shorter and wider than the posterior lobe, with a moderately developed ectostylid that is long and columnar (in labial view). Both protoconid and hypoconid have sharp labial angles. The lingual wall is relatively flat. The metaconid and entoconid swell bilaterally. The metastylid is large, mesostylid is very small and straight oriented; and the entostylid is large, distally oriented. In the lingual view, the crown is high. The metaconid and entoconid show upward apices. The columns of the metastylid, metaconid, entoconid, and entostylid are all clearly developed and columnar, with the former two being thick and the latter two being thin. The column of the mesostylid is not developed. The ectostylid is large and moderately high. The anterior lobe of m2 is partially visible. It shows broad anterior fossa with prominent spur anteriorly, protoconid, metaconid and its ribs while in the posterior lobe shows some part of entoconid.

The p4 (Fig. 4G), is in deep wear. The surface is marked by rugose enamel. In occlusal view, the shape is rectangular, with the length about twice the width (Table 2). The buccal wall is relatively flat. The mesolabial conid is rounded and the posterolabial conid shows a right angle. They are separated by a shallow groove. Due to wear, the groove between the anterior stylid and the anterior conid is indistinguishable. The mesolingual conid is distally inclined, leaving a broad V-shaped anterior valley; the posterior valley is a narrow U-shape while the back valley is narrow and slit like. The posterolingual conid and posterior stylid are slender and project prominently towards the lingual side, with the back valley extremely narrow. In the lingual view, the crown is high. The anterior valley and posterior valley extend to the crown base.

The m3 (Fig. 4H), is in moderate wear, with fine enamel rugosity. The apex of metaconid is damaged due to isotope sampling. The length is between two and three times the width. In occlusal view, all the cusps are triangular. For the protoconid, hypoconid, and hypoconulid, each has a triangular labial aspect. The preprotocristid and premetacristid merge mesially, showing a strong mesostyle; and the cristids between the first and the second lobes are interconnected in the middle. The ectostylid is broken above the base and shows a circular cross section. The metaconid swell bilaterally and the entoconid is only weakly inflated. The postentocristid and posthypocristid are not connected. The entoconulid is partially broken at the apex, very weak and separated from the hypoconulid through the back fossa of m3. Both metastylid and entostylid are moderately developed while the mesostylid is weak. In the lingual view, the crown is high. The anterior and posterior fossa are moderately broad. The ribs of the metaconid and the entoconid are columnar and slightly raised, the column of the mesostylid is distinct, forming a thin column. The entoconulid has a downward groove. A distinct carious trace is present at the base of metastylid.

5. Comparison and discussion

The horn core of the Shuitangba specimen is large, robust with a slight twist, sharp keels, and numerous short longitudinal grooves, while the cheek teeth are large, and hypsodont, where p3/dp3 and p4 are long and narrow, lack of anterior conid– mesolingual conid fusion resulting in broad and wide anterior valleys; anterior conid and anterior stylid separated by large groove, posterolingual conid and posterior stylid are also separate; rounded labial face due to the absence of posterolabial conid labial projection; in p4 mesolingual conid lingual face is only slightly extended anteriorly but very developed in the posterior direction, resulting in a kinked L-shape; in upper molars, entostyle tall and large which is attached throughout most of their length to the rest of the crown; mesostyles and metastyles projecting; fossae slightly complicated; while in lower molars ectostylids are tall and large; strong lingual ribs; m3 hypoconulid often buccally displaced having a wide connection to hypoconid. These dental characters are the diagnostic features for tribe Bovini given by Bibi (2007) and hence, are helpful to associate the described material with this tribe of subfamily Bovinae and exclude these from tribe Boselaphini specifically from Tragoportacini (e.g., *Tragoportax* and *Miotragocerus*) as these generally have smaller cheek teeth with lower crowns and less developed basal pillar (Bibi, 2007) and their horn cores are usually more flattened, with the horn base located near the midline of the frontal bone.

The basal Bovini from the Late Miocene deposits of Asia include two genera, *Pachyportax* and *Selenoportax* (Bibi, 2007, 2009). Both were originally described from the Siwalik Group of Indian subcontinent and are very close in their dental features (Pilgrim, 1939; Akhtar, 1992; Bibi, 2007; Khan et al., 2010; Gentry et al., 2014, 2025). Hence, both genera remain taxonomically debated, particularly regarding their dentition (Bibi, 2007; Gentry et al., 2014). This is specifically true for *S. lydekkeri* and *P. latidens* that have recently been considered as *nomina dubia* (Bibi, 2007) based on their holotypes but Bibi (2007) further added that "with regards to *P. latidens* especially, it would be appropriate to designate a neotype (ICZN Article 75.5), transferring the type of *P. latidens* from GSI-B219, the isolated M3, to GSI-B488 and B489, the skull Pilgrim (1937) designated as the type of *P. l. dhokpathanensis* (ICZN Article 61.4 applies)." Further, Bibi (2022a) while describing some specimens from Baynunah Formation, United Arab Emirates considered *P. latidens* valid. This and some other studies (e.g., Gentry, 1974, 1999; Nishioka et al., 2020) led to the synonymization of *P. latidens* and *P. l. dhokpathanensis* (contra Gentry et al., 2025, identifying *P. l. dhokpathanensis* as a distinct species (*P. dhokpathanensis*), resulting in overlapping in metric values. It is particularly evident in the metrics of dental elements attributed to different species of this genus, as the metrics show considerable variations even in the dentition allocated to a single species (Table 2). Nevertheless, such debate is beyond the scope of this study as it requires the study of whole Siwalik material of *Pachyportax* and *Selenoportax*. However, before we compare and discuss our specimens, it is better to provide a brief history of these two genera, highlighting the taxonomic problems of their species and determination of characters for better comparison.

Pachyportax was discovered near Hasnot, only including a single M3, which Lydekker (1876) identified as *Cervus latidens*. Then, Lydekker (1884) later classified it as *Oreas* (*Taurotragus*)? *latidens*. He further attributed teeth from Nila to *Oreas*? *latidens*, which were smaller than those from Hasnot, and showed some differences in detail features. Due to the different spatial distribution of these fossils, the larger morph type was named *Pachyportax latidens* (Pilgrim, 1937), and the smaller form was considered a variant of *P. latidens* and named *Pachyportax latidens* var. *dhokpathanensis* (Pilgrim, 1937, 1939). Pilgrim (1937) mentioned a fragment of a female *Pachyportax* skull found at Nagri, which was even smaller than *P. latidens dhokpathanensis* and named *Pachyportax nagrii*. However, it was not adequately distinguished from *Selenoportax vexillarius*, leading Gentry (1974, 1999) to question the validity of *P. nagrii*, and Nishioka et al. (2020) considered it an intraspecific variation of *P. latidens* but now considered a valid species by Gentry et al. (2025). Akhtar (1995) described and named a large sized species of *Pachyportax* from Dhok Pathan, named *P. giganteus*, which was soon transferred to *Selenoportax* (Bibi, 2009; Gentry et al., 2014; Nishioka et al., 2020). However, Nishioka et al. (2020) argued that it should remain in *Pachyportax*, besides the body size, *P. giganteus* and *P. latidens* show significant differences in horn core morphology. Gentry (1999) suggested that *Pachyportax* existed in the Siwalik region during the Nagri and Dhok Pathan formations and may have continued into the beginning of the Tatrot but was soon replaced by *Proamphibos*. However, this assertion should be further verified based on undisputed material.

Pilgrim (1937) first described the genus *Selenoportax*, and recognized two species *S. vexillarius* and *S. lydekkeri*. Initially, *S. vexillarius* was found in the Dhok Pathan type locality, while *S. lydekkeri* was found from both Dhok Pathan and Hasnot sites. Among them, *S. lydekkeri* was originally described as *Boselaphus lydekkeri* by Pilgrim (1910) and later transferred to the genus *Selenoportax*. A third species of the genus, *S. falconeri*, was originally described as *Boselaphus* sp. by Lydekker (1884), *Strepsiceros*(?) *falconeri* by Lydekker (1886), and finally *Perimia falconeri* by Pilgrim (1939). However, Nishioka et al. (2019) ascribed both *Perimia falconeri* and *S. lydekkeri* to *S. falconeri* based on the suggestions of Gentry et al. (2014). *S. falconeri* is now considered as a member of the genus *Pachyportax* (Gentry et al., 2025) though the horn core morphology shows that it should be treated as a species of the genus *Selenoportax* and we are treating it as a member of the genus *Selenoportax* in this study following (Nishioka et al., 2020) until its taxonomy is fully resolved. Later, Akhtar (1992), identified two more species, *Selenoportax dhokpathanensis* based on a skull, and *Selenoportax tatrotensis* based on a partial cranium with maxillae. Khan et al. (2009) synonymized *S. dhokpathanensis* with *S. lydekkeri* and *S. tatrotensis* with *S. vexillarius*.

Selenoportax and *Pachyportax* were initially classified within Boselaphini, but it was later recognized that they belong to the tribe Bovini based on careful assessment of the morphology and phylogenetic characteristics. Pilgrim (1937, p. 826) had already noted the similarity between the teeth of *Selenoportax* and *Pachyportax* and those of Bovini. According to Gentry (1974), *Strepsiportax gluten* (*Protragocerus gluten* in Gentry, 1974) gave rise to two evolutionary branches leading to *Selenoportax vexillarius* and *Pachyportax latidens*, respectively, with a possible brief transitional form *Helicoportax praecox* between *St. gluten* and *S. vexillarius*. Based on the Bovinae phylogenetic analysis of Bibi (2007, 2009), *Selenoportax* and *Pachyportax* are closely related. Pilgrim (1937) mentioned the similarity between *Pachyportax* and *Selenoportax*, particularly in the upper molars, which are very similar and difficult to distinguish. Bibi (2007) also suggested that the distinction between *Pachyportax* and *Selenoportax* cannot rely solely on the teeth but should be based on horn core and cranial characteristics. Specifically, specimens of *S. vexillarius* have never been found with both teeth and skull, making it impossible to ensure the true morphology.

Pilgrim (1937) highlighted the differences in horn cores: *Selenoportax* has a flatter medial surface and a convex lat-

eral surface, whereas *Pachyportax* has a convex inner side and a flatter outer side. Gentry (1974) identified three key differences in horn core morphology between *P. latidens* and *S. vexillarius*: *P. latidens* lacks a posteromedial keel, has an anterior keel not medially inserted, and a more laterally inclined horn core. However, the criteria proposed by Pilgrim (1937) and Gentry (1974) are somewhat ambiguous and difficult to apply in practice. Nishioka et al. (2020) proposed a more comprehensive method for distinguishing the two genera, mainly focusing on the horn core characters, such as the morphology of the supraorbital foramen, the angle of separation between the two horn cores, and the morphology of the horn core cross section (inward or outward compression/expansion), as well as some other characteristics such as body size.

Nevertheless, besides the size, the well preserved horn core cross section at the base could be another key source for taxonomic identification. In our specimen (ZYM ZT-2015-01461), the cross section of the horn core base is less compressed mediolaterally, with the medial surface being more bulged than the lateral surface (Fig. 5A). In *P. latidens*, the base of the horn core has a cross section that is less compressed mediolaterally, with a more bulged medial surface and a flatter lateral surface (Fig. 5B–D). In *P. giganteus*, the cross-section of the horn core base is similar to that of *P. latidens*, but it is strongly compressed mediolaterally and anteroposteriorly at the medial side (Fig. 5E). The medial surface is relatively more bulged than in *P. latidens*, and in some individuals, the medial surface may be nearly as bulged as the lateral surface, giving it an elongated oval shape. In *P. nagrii*, the anterior keel is prominent and sharp with a pronounced pinching near it while the posterior keel is weak and round, and the lateral side is much flatter than medial (Fig. 5F). In *S. vexillarius*, despite some variations, the cross section of the horn core at the base consistently displays a more bulged lateral surface, while the medial surface is essentially very flat (Fig. 5G). In *S. falconeri*, the horn core cross section at the base is generally more expanded mediolaterally, with approximately equal bulges on both the medial and lateral surfaces, giving it an olive shape (see Nishioka et al., 2020, fig. 5F, G). As a result, the Shuitangba specimen resembles *P. latidens* more than other species — both exhibit a relatively broad and blunt anterior profile with a slightly narrowed posterior profile but differs in having more ovoid cross section with less compressed lateral side and small size (Fig. 6).

The Zhaotong horn core also exhibits some characteristics that are different from all known species of *Selenoportax* and *Pachyportax*. For example, the horn cores from the Siwalik region, Myanmar, and Thailand of these two genera exhibit a distinct anterior medial and posterior lateral keel, whereas these keels are significantly reduced in the Zhaotong specimen; neither the horn core as a whole nor the keel in the Zhaotong specimen exhibits any pronounced torsion. Furthermore, Pilgrim (1947) proposed that the horn core cross sectional morphology of *Pachyportax* resembles that of the earliest buffalo lineage represented by *Proamphibos* and *Parabos*, suggesting an evolutionary relationship between *Pachyportax* and the early buffaloes. We observed that the cross section at the base of the horn core of the Zhaotong specimen exhibits more mediolateral expansion; and the distance between the orbit and the horn base has become relatively greater. These features may suggest a more advanced morphotype, showing some resemblance to the Pliocene genus *Proamphibos* and *Parabos*. However, they still exhibit significant differences. *Proamphibos* features a higher crown and a more complex occlusal surface structure with numerous small folds, and its horn cores have very sharp anterior medial and posterior lateral keels, with a third keel only becoming prominent in the upper part of the horn core. The cross section is relatively round, with swellings of both the lateral and medial surfaces, but the medial surface is even more swelled (Pilgrim, 1939). The European genus *Parabos* is considered to be very closely related to *Pachyportax* (Gentry, 1999; Lyras et al., 2022). The horn cores of *Parabos cordieri* are more upright, with a closer distance between the two horn cores, resulting in a smaller angle. The keels are reduced. The cross sectional shape transitions from nearly circular at the base to subtriangular in the middle, and then back to nearly circular at the distal end. Although the anterior and posterior keels are relatively weak, they are still present (Gromolard and Guerin, 1980). *Miotragocerus gregarius*, a member of the tribe Boselaphini, was distributed primarily in northern China during the Late Miocene. It is characterized by strongly backward curving horn cores bearing only anterior and posterior keels, exhibiting compressed elliptical or teardrop-shaped cross section (Shi and Zhang, 2023). The dentition of *M. gregarius* exhibits a squarish overall morphology, characterized by a well-developed and posteriorly positioned posterolingual cone on P3 and distinction between the anterolingual and posterolingual cones is not prominent, coupled with an anteroposteriorly expanded mesolingual conid on p4 (Zhang, 2005; Shi and Zhang, 2023). In contrast, the Shuitangba specimen differs markedly in both cranial and dental features: besides the overall large size and more hyposodont dentition, its horn cores lack the strong posterior curvature as seen in *M. gregarius* and display significantly different cross sectional morphology. The mandibular margin appears straighter, with less quadratic dental configuration. The P3 of the Shuitangba specimen exhibits a distinct posterolingual cone, but this structure is located anteriorly. On p4, the mesolingual conid lacks discernible anteroposterior expansion.

Zhaotong material may represent an intermediate evolutionary stage between *Pachyportax* and *Proamphibos*/*Parabos* and clearly constitutes a new species of *Pachyportax* that is more advanced than *P. latidens*. Since the weakening of the keels is an evolutionary trend from *Selenoportax* to *Pachyportax*, we argue that our material may belong to a more advanced and later morphotype of *Pachyportax*,

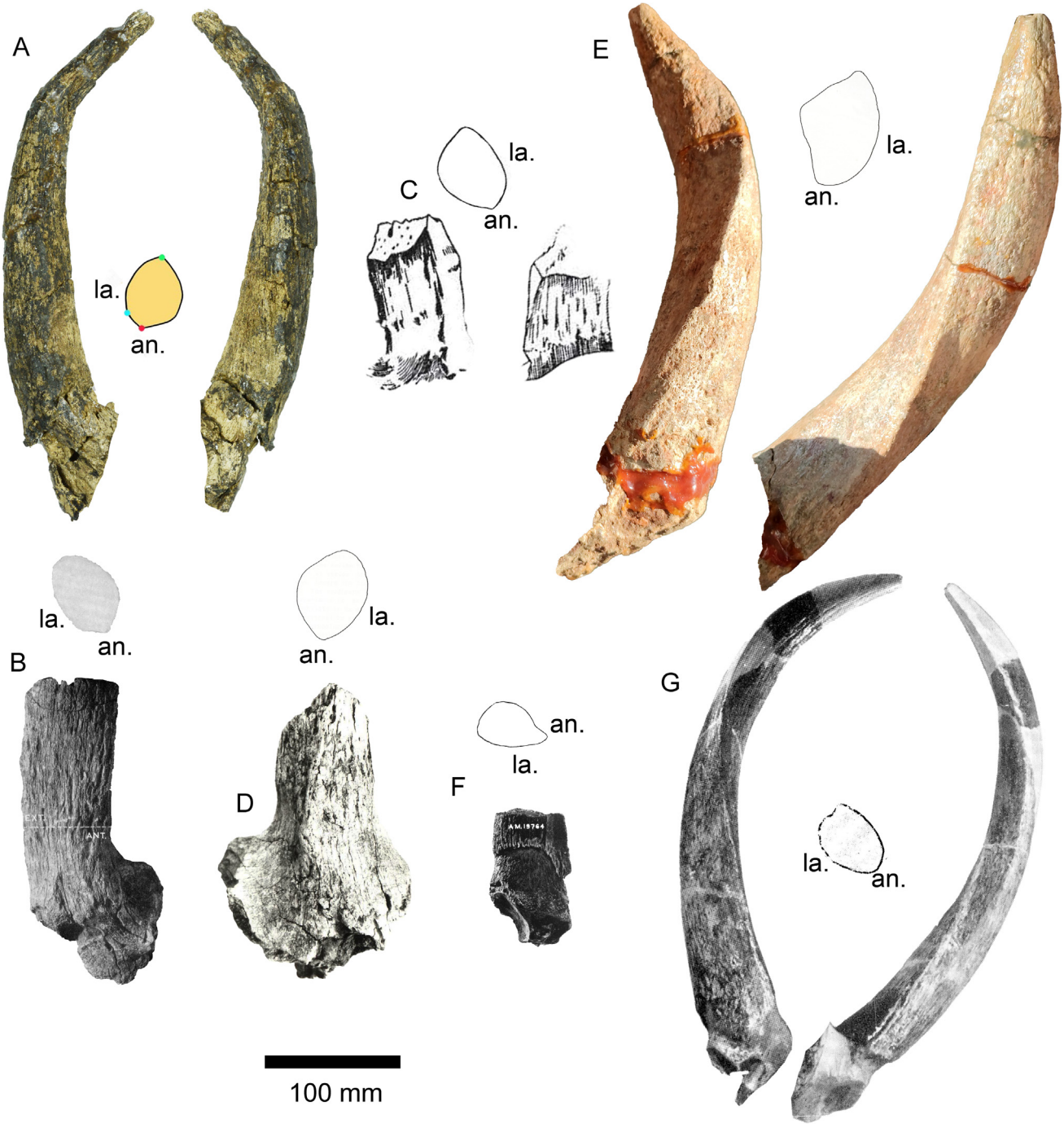

Fig.5. Comparison of horn cores of *Pachyportax* and *Selenoportax*. (A) *Pachyportax zhaotongensis* n. sp., ZYM ZT-2015-01461, right horn core in anterior and posterior views. (B) *P. latidens*, AMNH 9906, left horn core (Pilgrim, 1937) in anterior view. (C) *P. latidens*, GSI-B 488 (neotype), left horn corn (Pilgrim, 1939) in anterior and posterior views. (D) *P. latidens*, PUPC 85/103, left horn core (Akhtar, 1992) in anterior view. (E) *P. giganteus*, PUPC 87/323 (holotype), left horn core (Akhtar, 1992) in anterior and posterior views. (F) *P. nagrii*, AMNH 19764, base of right horn core (Pilgrim, 1937). (G) *Selenoportax vexillarius*, AMNH 19748 (holotype), right horn core (Pilgrim, 1937) in anterior and posterior views. Abbreviations: an, anterior; la, lateral.

and thus establish a new species *Pachyportax zhaotongensis* n. sp.

6. Cladistic analysis

Bayesian tip dating was performed based on morphological data (Fig. 7). In our reconstruction, *Pachyportax zhaotongensis* n. sp. is clustered with *Pachyportax latidens* with high support. *Pachyportax zhaotongensis* n. sp. and *P. latidens* form the sister group of all other taxa of Bovini except for the species of *Selenoportax*. The most recent common ancestor of *Pachyportax zhaotongensis* n. sp. and *P. latidens* is *Pachyportax giganteus* with a support of 40%. In the phylogenetic reconstruction by Bibi (2009), *Pachyportax* and *Selenoportax* form a sister group, but it also shows that *P. giganteus* is more closely related to

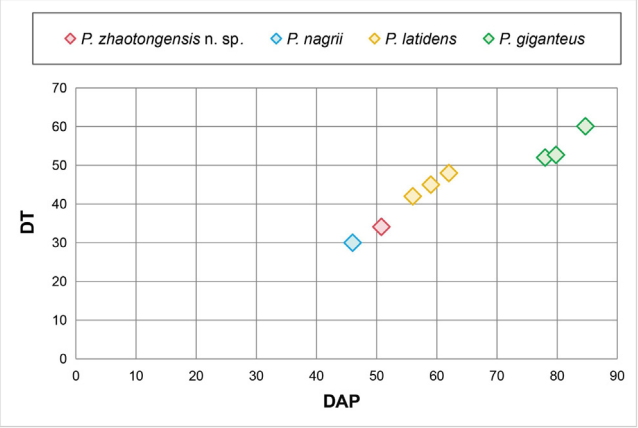

Fig. 6. Bivariate plot to illustrate the size differences among the various species of the genus *Pachyportax* based on Table 2.

Pachyportax than to *S. vexillarius* and *S. falconeri*. For a long time, the classification of *P. giganteus* — whether it belongs to *Selenoportax* or *Pachyportax* — has been subjected to debate. Our results place *P. giganteus* as an intermediate morphotype between *Selenoportax* and *Pachyportax*. Bibi (2009) suggested that *P. giganteus* represents a late stage morphotype of *Selenoportax*. From *S. vexillarius* to *S. falconeri* and then to *P. giganteus*, there is a progressive expansion and rounding of the medial surface in the cross section of the horn core at the base, ultimately evolving towards the more developed medial surface seen in *Pachyportax*. However, the morphology, size, and cladistic analysis done here do not support this suggestion and Gentry et al. (2025) also placed the species *giganteus* in the genus *Pachyportax*.

7. Discussion

The uplift of the Tibetan Plateau, resulting in the formation of the Himalayan barrier, separated the Oriental and Palaearctic realms. In the Late Miocene, *Selenoportax* and *Pachyportax* did not migrate northward to reach middle latitudes, as they were completely absent in the pan-Mediterranean region and northern China. However, they appeared in Southeast Asia and southern China, in which the fossil assemblages can be correlated to those of the Siwaliks (Eronen et al., 2009; Chavasseau et al., 2013; Flynn and Wessels, 2013; Flynn et al., 2013). Chavasseau et al. (2013) suggest that a sudden sea-level drop at 11 Ma leading to the dispersal of some Siwalik faunas to Southeast Asia, which was reflected in the faunal turnover in Myanmar (Haq et al., 1987; Takai et al., 2018). *Selenoportax* and *Pachyportax* may have also reach Southeast Asia and southern China in these faunal exchanges (Fig. 8). *Pachyportax* also dispersed to the Arabian region, as evidenced by fossils from the late Miocene Baynunah Formation in the United Arab Emirates (7.5–6.5 Ma) (Kingston, 1999; McDougall and Feibel, 2003; Bibi et al., 2013; Bibi, 2022b). Due to the closer relationship of the fauna with South Asia and Africa, Gentry (1999) considered the Baynunah fauna a "latitudinal differentiation fauna" connecting Africa and South Asia. *Pachyportax* from the Baynunah Formation is also a precursor for the large-scaled migration of Bovini to Africa in the Pliocene.

The rapid uplift of the Tibetan Plateau during the Late Neogene led to the gradual aridification of Central Asia, a trend that subsequently spread across much of Eurasia and Africa throughout the Late Cenozoic (Agustí et al., 2013; Yang et al., 2021). However, in Southeast Asia and southern China, including the Zhaotong region, the strengthening of the East Asian monsoon helped maintain a humid climate (Kaya, 2017; Kaya et al., 2018; Holbourn et al., 2021). Due to the combined effects of the Tibetan Plateau's uplift and the influence of the East Asian monsoon, Southeast Asia, including areas like Zhaotong in southern China, became climatically and geographically relatively isolated. This isolation delayed the global trend of drying and cooling, thus becoming a refuge for animals in the late Miocene. The skull fossil of a *Lufengpithecus* cf. *lufengensis*, dated to 6.2 Ma, discovered at Shuitangba in Zhaotong, Yunnan, is considered the youngest fossil of the fossil apes. In addition to *Lufengpithecus*, Shuitangba has yielded a highly diverse fauna adapted to a warm and humid environment, including fish, reptiles, birds, and mammals, among which the mammals comprise primates, talpids, soricids, erinaceids, carnivores, rodents, lagomorphs, perissodactyls, artiodactyls, and proboscideans (Jablonski et al., 2014). A recent molecular evolutionary study based on mitochondrial cytochrome b suggests that the radiation of Bovini began at about 12 Ma (Hassanin and Douzery, 1999), possibly in response to global climate changes during this period (Holbourn et al., 2021; Sun et al., 2024). Badgley et al. (2008) found that in the Siwalik region, mammalian faunal turnover rhythm coincided with shifts in vegetation: before 8.5 Ma, most herbivores fed on C_3 vegetation from closed forests; by 7 Ma herbivores primarily consumed C_3 plants, with a slight inclusion of C_4 grasses from woodland in a more open habitats; by 6.0 Ma, some herbivores had become mixed feeders, consuming both C_3 and C_4 plants, or were pure C_4 consumers (Quade et al., 1989; Morgan et al., 1994, 2009; Cande and Kent, 1995; Barry et al., 2002; Behrensmeyer et al., 2007). The diet of Bovini would have undergone a similar transition, and enamel stable isotope analysis of *Selenoportax* and *Pachyportax* samples from the Siwaliks during 8.3–7.9 Ma indicates a pure C_3 diet; however, the $\delta^{13}C$ values are positively biased, suggesting that they are potentially C_3 grazers (Bibi, 2007). In contrast, the $\delta^{13}C$ values of *Pachyportax* samples from around 7.3 Ma in the Siwaliks indicate that it had become a mixed feeder (Badgley et al., 2008). A similar dietary shift occurred in the Baynunah Formation of the Arabian region, where *P. latidens* was primarily a C_4 based mixed feeder (Bibi, 2022b), and in Myanmar, *S. vexillarius* was an obligate grazer and *S. falconeri* was a C_3/C_4 mixed feeder (Zin-Maung-Maung-Thein et al., 2011). However, the situation in the

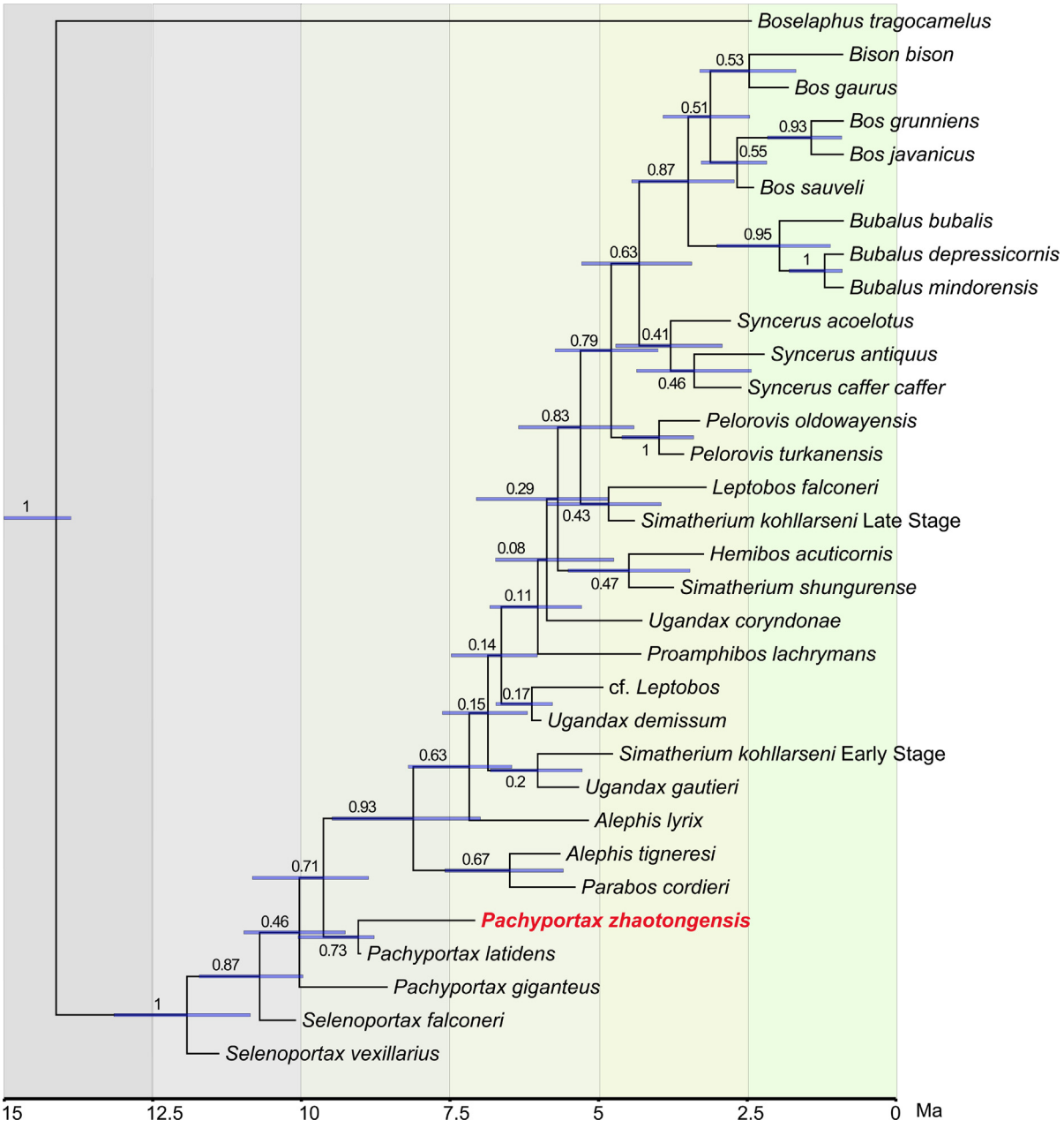

Fig. 7. Phylogenetic reconstruction of Bovini using Bayesian tip dating, taxa and characters follows Bibi (2009). The node support (the number at each node) is the posterior probability, and the node bars are 95% confidence age intervals. cf. *Leptobos* is cf. *Leptobos* cited as MNHNP no# in Bibi (2009).

Zhaotong Basin is different, where broad-leaved forests dominated during 7–6 Ma (Chang et al., 2015; Huang et al., 2017). Enamel stable isotope analysis sample from the P3 and P4 of the *P. zhaotongensis* n. sp. indicates that it was a pure C_3 feeder (Sun et al., 2021). Interestingly, *P. zhaotongensis* n. sp. shows the most negative $\delta^{13}C$ values among all mammals examined, suggesting that, unlike *Selenoportax* and *Pachyportax* from other regions, which show a transition to C_4 in their diet, *P. zhaotongensis* n. sp. remained an obligate browser that also consumed sugary content probably fruits in its diet. This is likely due to the closed forest environment of the Zhaotong Basin during this period (Sun et al., 2021). The abundant food sources in Zhaotong may have allowed *P. zhaotongensis* n. sp. to survive to a very late age.

8. Conclusions

The present study is focused on the first description of the genus *Pachyportax* from China based on the specimens collected from the Zhaotong Basin. The comparative study of the material revealed the presence of an advanced species of the genus that we named *Pachyportax zhaotongensis* n. sp. The horn core of this new species

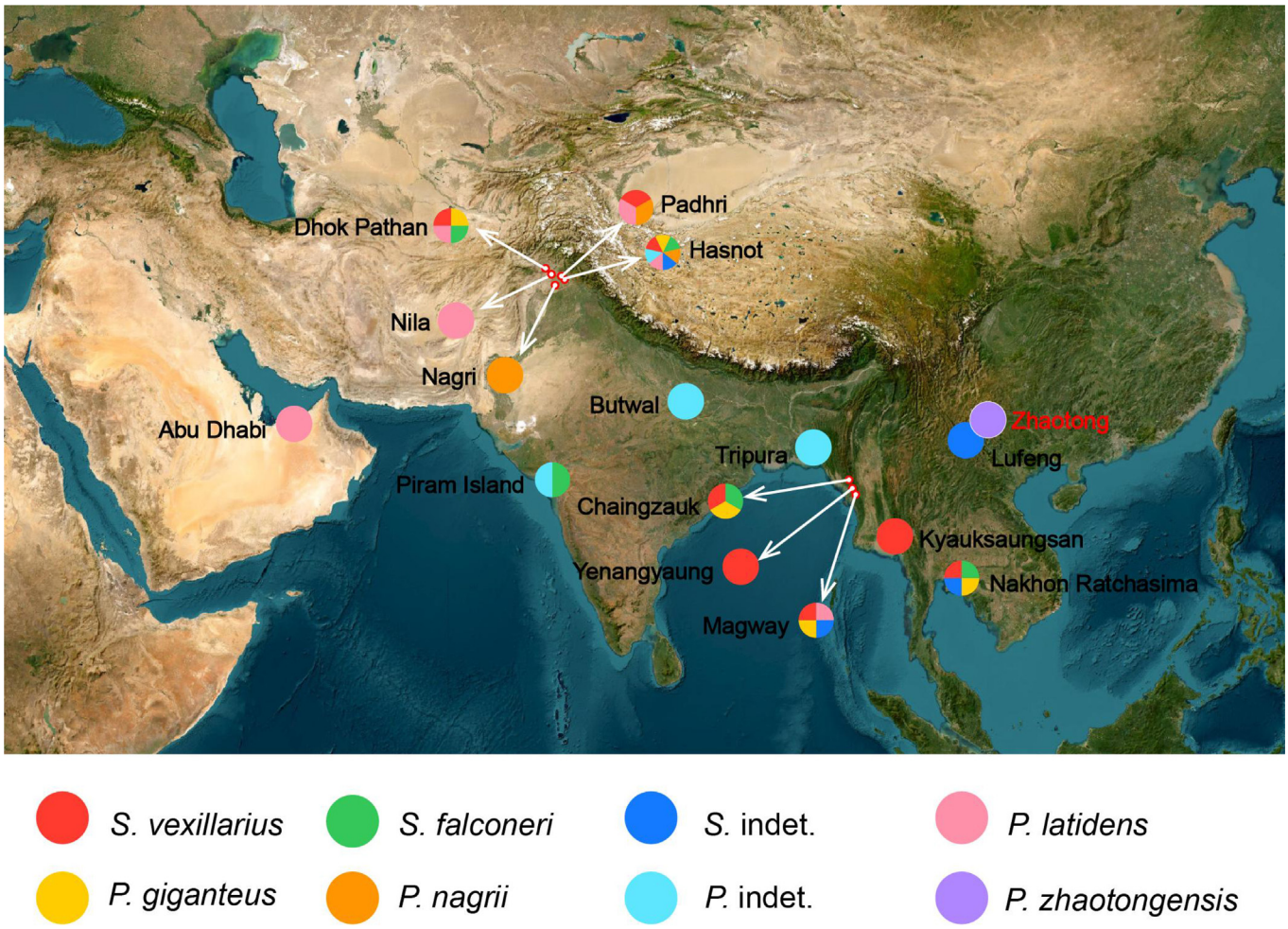

Fig. 8. Fossil localities of *Selenoportax* and *Pachyportax* in the world. The United Arab Emirates has one fossil site: Abu Dhabi; Pakistan has five fossil sites: Hasnot, Nila, Nagri, Padhri, and Dhok Pathan; India has two fossil sites: Piram Island and Tripura; Nepal has one fossil site: Butwal; Myanmar has four fossil sites: Chaingzauk, Yenangyaung, Magway, and Kyauksaungsan; Thailand has one fossil site: Nakhon Ratchasima; China has two fossil sites: Lufeng and Zhaotong.

shows less sharp keels, less flat lateral and more round medial side and less torsion unlike all the known species of the genus. Further, the phylogenetic analysis confirms the distinctness of *Pachyportax zhaotongensis* n. sp. and reveals that *Pachyportax* and *Selenoportax* are distinct genera. However, the taxonomic status of other species of both genera remain a subject of debate and further study is suggested. The new species described here is an obligate browser that was a C_3 feeder unlike the other species of the genus.

Declaration of competing interest

The authors declare that they have no known competing financial interests or personal relationships that could have appeared to influence the work reported in this paper.

Acknowledgements

We thank the curator, Jin Meng, from AMNH, for providing access to specimens for comparisons. We thank Xue-Lin Zhang, from Institute of Vertebrate Paleontology and Paleoanthropology, Chinese Academy of Sciences, for preparing the specimens. We are also grateful to Dr. Steven E. Jasinski for providing much needed literature and to Dr. Muhammad Adeeb Babar for his help in preparing figures. We thank the reviewers (Dr. Hao-Wen Tong and Prof. Dr. Muhammad Akhtar) for their constructive comments that improved the quality of the manuscript.

This work was supported by the National Key Research and Development Program of China (2023YFF0804501), the National Natural Science Foundation of China (No. 42430207, No. 42472004, No. 42402025) and the National Science Foundation of China (U23A26161, 42072209).

Supplementary data

Supplementary data to this article can be found online at https://doi.org/10.1016/j.palwor.2025.200996.

References

Abbas, S.G., Babar, M.A., Khan, M.A., Aftab, K., Riaz, A., Ghaffar, A., Akhtar, M., 2018. Fossil Bovidae from Late Miocene Dhok Pathan Formation of Siwaliks, Northern Pakistan. Pakistan Journal of Zoology 50 (1), 217–228.

Agustí, J., Cabrera, L., Garcés, M., 2013. The Vallesian Mammal Turnover: A Late Miocene record of decoupled land-ocean evolution. Geobios 46 (1–2), 151–157.

Akhtar, M., 1992. Taxonomy and distribution of the Siwalik bovid. PhD Dissertation, University of the Punjab, Lahore, Pakistan, 372 pp.

Akhtar, M., 1995. *Pachyportax giganteus*, new species (Mammalia: Artiodactyla: Bovidae) from the Dhok Pathan, district Chakwal, Punjab, Pakistan. Pakistan Journal of Zoology 27, 337–340.

Babar, M.A., Aftab, K., Khan, M.A., Batool, T., Abbas, S.G., Shahid, R., Akhtar, M., 2018. *Pachyportax* (Bovidae: Ruminantia) from Dhok Pathan Formation of Siwaliks. The Journal of Animal and Plant Sciences 28 (2), 508–514.

Badgley, C., Barry, J.C., Morgan, M.E., Nelson, S.V., Behrensmeyer, A. K., Cerling, T.E., Pilbeam, D., 2008. Ecological changes in Miocene mammalian record show impact of prolonged climatic forcing. Proceedings of the National Academy of Sciences of the United States of America 105 (34), 12145–12149.

Bärmann, E.V., Rössner, G.E., 2011. Dental nomenclature in Ruminantia: Towards a standard terminological framework. Mammalian Biology 76, 762–768.

Barry, J.C., Morgan, M.E., Flynn, L.J., Pilbeam, D., Behrensmeyer, A.K., Raza, S.M., Khan, I.A., Badgley, C., Hicks, J., Kelley, J., 2002. Faunal and environmental change in the late Miocene Siwaliks of northern Pakistan. Paleobiology 28, 1–71.

Behrensmeyer, A.K., Quade, J., Cerling, T.E., Kappelman, J., Khan, I.A., Copeland, P., Roe, L., Hicks, J., Stubblefield, P., Willis, B.J., 2007. The structure and rate of late Miocene expansion of C_4 plants: Evidence from lateral variation in stable isotopes in paleosols of the Siwalik Group, northern Pakistan. Geological Society of America Bulletin 119, 1486–1505.

Bibi, F., 2007. Origin, paleoecology, and paleobiogeography of early Bovini. Palaeogeography, Palaeoclimatology, Palaeoecology 248 (1–2), 60–72.

Bibi, F., 2009. Evolution, systematics, and paleoecology of Bovinae (Mammalia: Artiodactyla) from the Late Miocene to the Recent. PhD Dissertation, Yale University, New Haven, Connecticut, 469 pp.

Bibi, F., 2013. A multi-calibrated mitochondrial phylogeny of extant Bovidae (Artiodactyla, Ruminantia) and the importance of the fossil record to systematics. BMC Evolutionary Biology 13, 166.

Bibi, F., 2022a. Bovidae and Giraffidae from the Baynunah Formation. In: Bibi, F., Kraatz, B., Beech, M.J., Hill, A. (Eds.), Sands of Time: Ancient Life in the Late Miocene of Abu Dhabi, United Arab Emirates. Springer Nature, Cham, pp. 219–244.

Bibi, F., 2022b. Stable isotope paleoecology of the Baynunah Formation. In: Bibi, F., Kraatz, B., Beech, M.J., Hill, A. (Eds.), Sands of Time: Ancient Life in the Late Miocene of Abu Dhabi, United Arab Emirates. Springer Nature, Cham, pp. 299–331.

Bibi, F., Maia, B., Gentry, A.W., Geraads, K.D.S., Vrba, E.S., 2009. The fossil record and evolution of Bovidae: state of the field. Palaeontologia Electronica 12, Article number 12.3.10A.

Bibi, F., Hill, A., Beech, M., Yasin, W., 2013. Chapter 27. Late Miocene fossils from the Baynunah Formation, United Arab Emirates: Summary of a decade of new work. In: Wang, X., Flynn, L.J., Fortelius, M. (Eds.), Fossil Mammals of Asia: Neogene Biostratigraphy and Chronology. Columbia University Press, New York, pp. 583–594.

Cande, S.C., Kent, D.V., 1995. Revised calibration of the geomagnetic polarity timescale for the Late Cretaceous and Cenozoic. Journal of Geophysical Research: Solid Earth 100, 6093–6095.

Chang, L., Guo, Z., Deng, C., Wu, H., Ji, X., Zhao, Y., Zhang, C., Ge, J., Wu, B., Sun, L., 2015. Pollen evidence of the palaeoenvironments of *Lufengpithecus lufengensis* in the Zhaotong Basin, southeastern margin of the Tibetan Plateau. Palaeogeography, Palaeoclimatology, Palaeoecology 435 (1), 95–104.

Chavasseau, O., Khyaw, A.A., Chaimanee, Y., Coster, P., Emonet, E.G., Soe, A.N., Rugbumrung, M., Tun, S.T., Jaeger, J.J., 2013. Advances in the biochronology and biostratigraphy of the continental Neogene of Myanmar. In: Wang, X., Flynn, L.J., Fortelius, M. (Eds.), Fossil Mammals of Asia: Neogene Biostratigraphy and Chronology. Columbia University Press, New York, pp. 461–474.

Eronen, J.T., Ataabadi, M.M., Micheels, A., Karme, A., Bernor, R.L., Fortelius, M., 2009. Distribution history and climatic controls of the Late Miocene Pikermian chronofauna. Proceedings of the National Academy of Sciences of the United States of America 106 (29), 11867–11871.

Flynn, L.J., Wessels, W., 2013. Paleobiogeography and South Asian small mammals: Neogene latitudinal faunal variation. In: Wang, X., Flynn, L.J., Fortelius, M. (Eds.), Fossil Mammals of Asia: Neogene Biostratigraphy and Chronology. Columbia University Press, New York, pp. 445–460.

Flynn, L., Lindsay, E., Pilbeam, D., Raza, S., Morgan, M., Barry, J., Badgley, C., Behrensmeyer, A., Cheema, I., Rajpar, A., 2013. The Siwaliks and Neogene evolutionary biology in South Asia. In: Wang, X., Flynn, L.J., Fortelius, M. (Eds.), Fossil Mammals of Asia: Neogene Biostratigraphy and Chronology. Columbia University Press, New York, pp. 353–372.

Froese, D., Stiller, M., Heintzman, P.D., Reyes, A.V., Zazula, G.D., Soares, A.E., Meyer, M., Hall, E., Jensen, B.J., Arnold, L.J., 2017. Fossil and genomic evidence constrains the timing of bison arrival in North America. Proceedings of the National Academy of Sciences of the United States of America 114 (13), 3457–3462.

Gavryushkina, A., Welch, D., Stadler, T., Drummond, A.J., 2014. Bayesian inference of sampled ancestor trees for epidemiology and fossil calibration. PLoS Computational Biology 10, e1003919.

Gentry, A.W., 1974. A new genus and species of Pliocene boselaphine (Bovidae, Mammalia) from South Africa. Annals of the South African Museum 65, 145–188.

Gentry, A.W., 1999. Fossil Pecorans from the Baynunah Formation, Emirate of Abu Dhabi, United Arab Emirates. In: Whybrow, P.J., Hill, A. (Eds.), Fossil Vertebrates of Arabia. Yale University Press, New Haven, pp. 290–316.

Gentry, A.W., Gentry, A., 1978. Fossil Bovidae (Mammalia) of Olduvai Gorge, Tanzania. Bulletin of the British Museum (Natural History) Geology 29 (4), 289–446.

Gentry, A.W., Rössner, G.E., Heizmann, E.P.J., 1999. Suborder Ruminantia. In: Rössner, G.E., Heissig, K. (Eds.), The Miocene Land Mammals of Europe. Verlag Friedrich Pfeil, Munich, pp. 225–258.

Gentry, A.W., Solounias, N., Barry, J.C., 2014. Stability in higher level taxonomy of Miocene bovid faunas of the Siwaliks. Annales Zoologici Fennici 51, 49–56.

Gentry, A.W., Solounias, N., Barry, J.C., 2025. Siwalik Bovidae. In: Badgley, C., Morgan, M.E., Pilbeam, D. (Eds.), At the Foot of the Himalayas: Paleontology and Ecosystem Dynamics of the Siwalik Record. Johns Hopkins University Press, Baltimore, pp. 368–388.

Geyer, C.J., 1992. Practical Markov Chain Monte Carlo. Statistical Science 7, 473–483.

Gray, J.E., 1821. On the natural arrangement of vertebrose animals. London Medical Repository 15, 296–310.

Gromolard, C., Guerin, C., 1980. Mise au point sur *Parabos cordieri* (de Christol), un Bovide (Mammalia, Artiodactyla) du Pliocene d'Europe occidentale. Geobios 13 (5), 741–755.

Han, D.F., 1985. The Artiodactyla of *Ramapithecus* site, Lufeng, Yunnan. Acta Anthropologica Sinica 4 (1), 44–54 (in Chinese, with English abstract).

Haq, B.U., Hardenbol, J., Vail, P.R., 1987. Chronology of fluctuating sea levels since the Triassic. Science 235, 1156–1167.

Harris, J.M., 2003. 2. Bovidae from the Lothagam Succession. In: Leaky, M.G., Harris, J.M. (Eds.), Lothagam: The Dawn of Humanity in Eastern Africa. Columbia University Press, New York, pp. 531–580.

Hassanin, A., Douzery, E.J., 1999. The tribal radiation of the family Bovidae (Artiodactyla) and the evolution of the mitochondrial cytochrome b gene. Molecular Phylogenetics and Evolution 13, 227–243.

Heath, T.A., Huelsenbeck, J.P., Stadler, T., 2014. The fossilized birth-death process for coherent calibration of divergence-time estimates. Proceedings of the National Academy of Sciences of the United States of America 111, E2957–E2966.

Holbourn, A., Kuhnt, W., Clemens, S.C., Heslop, D., 2021. A ~12 myr Miocene record of East Asian monsoon variability from the South China Sea. Paleoceanography and Paleoclimatology 36, e2021PA004267.

Huang, Y.J., Ji, X.P., Su, T., Deng, C.L., Ferguson, D.K., Yu, T.S., Yang, X., Sun, H., Zhou, Z.K., 2017. Habitat, climate and potential plant food resources for the Late Miocene Shuitangba hominoid in Southwest China: Insights from carpological remains. Palaeogeography, Palaeoclimatology, Palaeoecology 470 (15), 63–71.

Jablonski, N.G., Su, D.F., Flynn, L.J., Ji, X.P., Deng, C.L., Kelley, J., Zhang, Y.G., Yin, J.Y., You, Y.S., Yang, X., 2014. The site of Shuitangba (Yunnan, China) preserves a unique, terminal Miocene fauna. Journal of Vertebrate Paleontology 34, 1251–1257.

Ji, X., Jablonski, N.G., Su, D.F., Deng, C., Flynn, L.J., You, Y., Kelley, J., 2013. Juvenile hominoid cranium from the terminal Miocene of Yunnan, China. Chinese Science Bulletin 58 (31), 3771–3779.

Kaya, F., 2017. Paleobiogeographic and Paleoecologic Development of the Old World Savanna Paleobiome during the Neogene. PhD Dissertation, University of Helsinki, Helsinki, 56 pp.

Kaya, F., Bibi, F., Žliobaitė, I., Eronen, J.T., Hui, T., Fortelius, M., 2018. The rise and fall of the Old World savannah fauna and the origins of the African savannah biome. Nature Ecology & Evolution 2, 241–246.

Khan, M.A., Iliopoulos, G., Akhtar, M., 2009. Boselaphines (Artiodactyla, Ruminantia, Bovidae) from the Middle Siwaliks of Hasnot, Pakistan. Geobios 42 (6), 739–753.

Khan, M., Akhtar, M., Iqbal, M., 2010. The late Miocene artiodactyls in the Dhok Pathan type locality of the Dhok Pathan formation, the Middle Siwaliks, Pakistan. Pakistan Journal of Zoology Supplementary Series 10, 1–90.

Khan, M.A., Akhtar, M., Ikram, T., 2012. True ungulates from the Nagri type locality (Late Miocene), northern Pakistan. The Journal of Animal and Plant Sciences Supplementary Series 22, 1–59.

Kingston, J., 1999. Isotopes and environments of the Baynunah Formation, Emirate of Abu Dhabi, United Arab Emirates. In: Whybrow, P. J., Hill, A. (Eds.), Fossil Vertebrates of Arabia. Yale University Press, New Haven, pp. 354–372.

Lepage, T., Bryant, D., Philippe, H., Lartillot, N., 2007. A general comparison of relaxed molecular clock models. Molecular Biology and Evolution 24, 2669–2680.

Lewis, P.O., 2001. A likelihood approach to estimating phylogeny from discrete morphological character data. Systematic Biology 50, 913–925.

Lydekker, R., 1876. Molar teeth and other remains of Mammalia. Records of the Geological Survey of India 10, 1–87.

Lydekker, R., 1884. Indian Tertiary and post-Tertiary Vertebrata. Rodents and new ruminants from the Siwaliks, and synopsis of Mammalia. Memoirs of the Geological Survey of India 10 (3), 105–134.

Lydekker, R., 1886. Siwalik Mammalia, supplement I. Palaeontologia Indica 10 (1), 1–21.

Lyman, R.L., 2004. Late-Quaternary diminution and abundance of prehistoric bison (*Bison* sp.) in eastern Washington state, USA. Quaternary Research 62 (1), 76–85.

Lyras, G.A., Athanassiou, A., van der Geer, A.A., 2022. The fossil record of insular endemic mammals from Greece. In: Vlachos, E., Herridge, V. (Eds.), Fossil Vertebrates of Greece Vol. 2: Laurasiatherians, Artiodactyles, Perissodactyles, Carnivorans, and Island Endemics. Springer Nature, Cham, pp. 661–701.

Martínez-Navarro, B., Palombo, M.R., 2004. Occurrence of the Indian genus *Hemibos* (Bovini, Bovidae, Mammalia) at the Early–Middle Pleistocene transition in Italy. Quaternary Research 61 (3), 314–317.

Martínez-Navarro, B., Ros-Montoya, S., Espigares, M.P., Palmqvist, P., 2011. Presence of the Asian origin Bovini, *Hemibos* sp. aff. *Hemibos gracilis* and *Bison* sp., at the early Pleistocene site of Venta Micena (Orce, Spain). Quaternary International 243, 54–60.

McDougall, I., Feibel, C.S., 2003. 3. Numerical age control for the Miocene–Pliocene succession at Lothagam, a Hominoid-bearing sequence in the Northern Kenya Rift. In: Leaky, M.G., Harris, J.M. (Eds.), Lothagam: The Dawn of Humanity in Eastern Africa. Columbia University Press, New York, pp. 43–64.

Morgan, M.E., Kingston, J.D., Marino, B.D., 1994. Carbon isotopic evidence for the emergence of C_4 plants in the Neogene from Pakistan and Kenya. Nature 367, 162–165.

Morgan, M.E., Behrensmeyer, A.K., Badgley, C., Barry, J.C., Nelson, S., Pilbeam, D., 2009. Lateral trends in carbon isotope ratios reveal a Miocene vegetation gradient in the Siwaliks of Pakistan. Geology 37 (2), 103–106.

Nishioka, Y., Takai, M., Tsubamoto, T., Egi, N., Nishimura, T., Kono, R., Ogino, S., Vidthayanon, C., 2019. Bovidae (Mammalia, artiodactyla) from the Neogene Irrawaddy beds, Myanmar. Palaeontographica, Abteilung A: Palaozoologie - Stratigraphie 314, 11–68.

Nishioka, Y., Vidthayanon, C., Hanta, R., Duangkrayom, J., Jintasakul, P., 2020. Neogene Bovidae from Tha Chang Sandpits, Nakhon Ratchasima, Northeastern Thailand. The Thailand Natural History Museum Journal 14, 59–71.

Pilgrim, G.E., 1910. Notices of new mammalian genera and species from the Tertiaries of India. Records of the Geological Survey of India 40, 63–71.

Pilgrim, G.E., 1937. Siwalik antelopes and oxen in the American Museum of Natural History. Bulletin of the American Museum of Natural History 72 (7), 729–874.

Pilgrim, G.E., 1939. The fossil Bovidae of India. Palaeontologica Indica 26, 1–356.

Pilgrim, G.E., 1947. The evolution of the buffaloes, oxen, sheep and goats. Zoological Journal of the Linnean Society 41 (279), 272–286.

Qiu, Z., Qiu, Z., 1995. Chronological sequence and subdivision of Chinese Neogene mammalian faunas. Palaeogeography, Palaeoclimatology, Palaeoecology 116 (1–2), 41–70.

Quade, J., Cerling, T.E., Bowman, J.R., 1989. Development of Asian monsoon revealed by marked ecological shift during the latest Miocene in northern Pakistan. Nature 342, 163–166.

Renfrew, C., 2006. Inception of agriculture and rearing in the Middle East. Comptes Rendus Palevol 5, 395–404.

Ronquist, F., Klopfstein, S., Vilhelmsen, L., Schulmeister, S., Murray, D. L., Rasnitsyn, A.P., 2012a. A total-evidence approach to dating with fossils, applied to the early radiation of the Hymenoptera. Systematic Biology 61, 973–999.

Ronquist, F., Teslenko, M., van der Mark, P., Ayres, D.L., Darling, A., Höhna, S., Larget, B., Liu, L., Suchard, M.A., Huelsenbeck, J.P., 2012b. MrBayes 3.2: Efficient Bayesian phylogenetic inference and model choice across a large model space. Systematic Biology 61, 539–542.

Shi, Q.Q., Zhang, Z.Q., 2023. New material of *Miotragocerus* (Bovidae, Artiodactyla) from northern China and its systematic implications. Journal of Systematic Palaeontology 21 (1), 2194891.

Siddiq, M.K., Khan, M.A., Akhtar, M., 2016. *Bos* (Mammalia: Bovidae) from the Pinjor Formation of Sardhok, Pakistan. Pakistan Journal of Zoology 48, 1071–1075.

Stadler, T., 2010. Sampling-through-time in birth–death trees. Journal of Theoretical Biology 267, 396–404.

Sun, F.J., Wang, Y., Jablonski, N.G., Hou, S.K., Ji, X.P., Wolff, B., Tripati, A., Cao, J.Y., Yang, X., 2021. Paleoenvironment of the Late Miocene Shuitangba hominoids from Yunnan, Southwest China: Insights from stable isotopes. Chemical Geology 569, 120–123.

Sun, J.M., Sha, J.G., Wang, S.Q., 2024. Stepwise closure of the Tethyan Seaway and its impact on the Earth's multi-sphere interactions during the Cenozoic. Chinese Science Bulletin 69 (2), 184–199 (in Chinese, with English abstract).

Takai, M., Kusuhashi, N., Nishioka, Y., Thaung, H., Zin-Maung-Maung-Thein, 2018. Geological setting and transition of the Neogene mammal fauna in central Myanmar. Fossils 103, 5–20.

Tong, H.W., Chen, X., Zhang, B., 2017. New fossils of *Bison palaeosinensis* (Artiodactyla, Mammalia) from the steppe mammoth site of Early Pleistocene in Nihewan Basin, China. Quaternary International 445, 250–268.

Yang, Y., Ye, C., Galy, A., Fang, X., Xue, Y., Liu, Y., Yang, R., Zhang, R., Han, W., Zhang, W., 2021. Monsoon-enhanced silicate weathering as a new atmospheric CO_2 consumption mechanism contributing to fast Late Miocene global cooling. Paleoceanography and Paleoclimatology 36, e2020PA004008.

Yang, Z., 1994. Maximum likelihood phylogenetic estimation from DNA sequences with variable rates over sites: approximate methods. Journal of Molecular Evolution 39, 306–314.

Zhang, C., Guo, Z., Deng, C., Ji, X., Wu, H., Paterson, G.A., Chang, L., Li, Q., Wu, B., Zhu, R., 2016a. Clay mineralogy indicates a mildly warm and humid living environment for the Miocene hominoid from the Zhaotong Basin, Yunnan, China. Scientific Reports 6, 20012.

Zhang, C., Stadler, T., Klopfstein, S., Heath, T.A., Ronquist, F., 2016b. Total-evidence dating under the fossilized birth–death process. Systematic Biology 65, 228–249.

Zhang, K., Lenstra, J., Zhang, S., Liu, W., Liu, J., 2020. Evolution and domestication of the Bovini species. Animal Genetics 51 (5), 637–657.

Zhang, Z., 2005. Late Miocene Boselaphini (Bovidae, Artiodactyla) from Fugu, Shaanxi Province, China. Vertebrata Palasiatica 43, 208–218.

Zin-Maung-Maung-Thein, Takai, M., Uno, H., Wynn, J.G., Egi, N., Tsubamoto, T., Nishimura, T., Yoneda, M., 2011. Stable isotope analysis of the tooth enamel of Chaingzauk mammalian fauna (late Neogene, Myanmar) and its implication to paleoenvironment and paleogeography. Palaeogeography, Palaeoclimatology, Palaeoecology 300 (1–4), 11–22.